The Effects of Simple Objects on the Electric Field of *Apteronotus*

Brian Rasnow

Division of Biology, California Institute of Technology, 216-76, Pasadena, CA 91125 USA

Summary. How might electric fish determine, from patterns of transdermal voltage changes, the size, shape, location, and impedance of a nearby object? I have investigated this question by measuring and simulating "electric images" of spheres and ellipsoids near an *Apteronotus leptorhynchus*. Previous studies have shown that this fish's electric field magnitude, and perturbations of the field due to objects, are complicated nonlinear functions of distance from the fish. These functions become much simpler when distance is measured from the axes of symmetry of the fish and the object, instead of their respective edges. My analysis suggests the following characteristics of high frequency electric sense and electric images. 1. The shape of electric images on the fish's body is relatively independent of a spherical object's radius, conductivity, and rostrocaudal location. 2. An image's relative width increases linearly with lateral distance, and might therefore unambiguously encode object distance. 3. Only objects with very large dielectric constants cause appreciable phase shifts, and the degree of shift depends strongly on water conductivity. 4. Several parameters, such as the range of electric sense, may depend on the rostrocaudal location of an object. Large objects may be detectable further from the head than the tail, and conversely, small objects may be detectable further from the tail than head. 5. Asymmetrical objects produce different electric images, correlated with their cross-sections, for different orientations and phases of the electric field. 6. The steep attenuation with distance of the field magnitude causes spatial distortions in electric images, somewhat analogous to the perspective distortion inherent in wide angle optical lenses.

Key words: Electrolocation – Electroreception – Weakly electric fish – *Apteronotus*

Introduction

Several diverse groups of animals possess sensory systems specialized for detecting weak electric fields (reviewed in Bastian 1994). Electric fields permeate aquatic environments, arising from neuronal and muscle activity, and even the motion of the animal in the geomagnetic field (Kalmijn 1986; Paulin 1995). Two orders of freshwater fish have extended their electric sensory abilities by actively generating a stable, high frequency, weak electric field (0.1-10 kHz, ≤ 100 mV/cm) known as the electric organ discharge (EOD; Bennett 1971). These "weakly electric fish" have thousands of receptor organs in their skin that are tuned and exquisitely sensitive to EOD modulations caused by nearby objects with different impedance than the surrounding water (Bastian 1981). Weakly electric fish are extremely productive model systems for studying sensory and motor neural systems (Heiligenberg & Bullock 1986).

In a companion paper, Rasnow and Bower (1996) presented high spatial and temporal resolution maps of the electric field generated by the weakly electric fish, *Apteronotus leptorhynchus*. Here I explore how the fish's electric field is perturbed by objects, and how the fish might perceive and identify objects based on the pattern of these "object perturbations", or "electric images". I derived electric images of objects using two complementary methods. First, I directly measured the electric potential between small electrodes placed against the fish's skin and a distant reference electrode, while a metal sphere was positioned at various distances from the fish. The image was computed as the difference between the potential with and without the object present. A second approach was to mathematically simulate electric images of small objects. The simulations were based on electric field vector measurements in the absence of objects (Rasnow and Bower 1996), combined with an analytic model of the object.

An object placed in an electric field will develop a surface charge distribution in response to the field. If the object and field are symmetrical and homogeneous, an analytic solution may be found for the induced charge and the resulting field perturbation. For example, the perturbation due to a homogeneous sphere in a uniform field is purely dipolar and proportional to the unperturbed field (see Appendix). An object perturbation is much weaker than the unperturbed field, and its measurement by the first method above is susceptible to a number of systematic errors. The simulations, in contrast, are more robust to measurement errors (see Discussion). Furthermore, because the object is modeled analytically, the simulations provide insight into the parameters and functional dependencies that affect electric images.

Electric images can be described either as perturbations of the electric field or of the electric potential at the skin. The electroreceptor organs most likely respond to the

Abbreviations: EOD, electric organ discharge; EO, electric organ; RMS, root-mean-square; p-p, peak-to-peak; e, eccentricity.

potential across their active membranes (Bennett and Shosaku 1986). A nearby object has greater effect on the potential outside a fish than internally, because the high impedance of the skin relative to the interior acts as a voltage divider, dropping most of the perturbation voltage over the skin (see Discussion). Therefore, to a first order approximation, the electric image of a nearby object can be described by the resulting change in potential at the skin surface. Although only potential perturbations were measured on the skin, the simulator can compute changes in both the potential and current.

Objects may modulate both the EOD amplitude and phase. Electric fish are sensitive to both these parameters, and have separate receptor organs and neural pathways specialized for processing each component (Carr, 1990; Scheich et al. 1973). In this study, I focus on the input to the amplitude pathway. Amplitude coding receptors or P-units in *Apteronotus* modulate their probability of firing as a function of EOD amplitude (e.g., Nelson et al. 1993). Precisely how the EOD signal is rectified and integrated by these receptors is still being investigated. For this reason, I assume a simple transfer function for the receptors: the change in root-mean-square (RMS) amplitude. However, my conclusions do not depend on the detailed functional form of the transfer function.

Methods

These measurements were conducted on the same individual *A. leptorhynchus*, and during the same recording session as described in Rasnow and Bower (1996). The recording and analysis methods are described in detail in Rasnow (1994). The coordinate system has origin at the mouth and is oriented with basis vectors rostral, lateral, and dorsal.

Measurements of electric images. The potential on the fish's skin was measured with a flexible linear array of five silver ball electrodes approximately 5 mm apart (a similar array is shown in Rasnow et al. 1993, Fig. 1B). Each electrode was insulated to its tip, which was approximately a 200 μm diameter sphere. Potentials were measured relative to a 1 mm diameter silver electrode mounted on the tank wall 30 cm lateral of the fish. Because the object was opaque, the following sequence was used to position the object over the electrode array. The electrodes were placed on the approximate dorsoventral midline and their locations were recorded by a video camera lateral of the fish. The array was then removed and the object, a 2.2 cm diameter brass sphere attached to a manipulator, was placed in contact with the skin to calibrate its lateral distance. The object was moved 2 mm lateral and the electrode array was repositioned against the skin. Measurements were taken as the object was stepped away from the fish. The sequence of object distances was repeated twice at three locations along the rostro-caudal axis, and once at a more caudal location.

Simulations of electric images of spheres. A sphere of radius *a* placed in a uniform electric field $\mathbf{E}_0$ generates a purely dipolar potential proportional to the field. For the simulations presented here, I assumed the electric field was uniform and equal to the value measured at the object's center (before placing the object there). At a position $\mathbf{r}$ from the object center, the perturbation is given by (see Appendix for derivation):

$$\delta\varphi(\mathbf{r}) = \mathbf{E}_0 \cdot \mathbf{r}\left(\frac{a}{r}\right)^3 \frac{\rho_1 - \rho_2 + i\omega\rho_1\rho_2(\varepsilon_2 - \varepsilon_1)}{2\rho_2 + \rho_1 + i\omega\rho_1\rho_2(2\varepsilon_1 + \varepsilon_2)} \quad (1)$$

where ρ_1 = 5 kΩ-cm is the resistivity of the water; $\varepsilon_1 \cong 80\varepsilon_0 \cong 7.1$ pF/cm is the dielectric constant of water; ρ_2 and ε_2 are the resistivity and dielectric strength of the spherical object of radius *a*; $\omega = 2\pi f$ is the angular frequency of the unperturbed electric field, $\mathbf{E}_0=(E_{0r}, E_{0l}, E_{0d})$; $r = |\mathbf{r}|$ (the length of the position vector, $\mathbf{r}$); and $i = \sqrt{-1}$. The simulation was run independently for the ten lowest order EOD harmonics. Waveforms were computed by the inverse Fourier transform of the superposition of these harmonics.

For a perfectly conducting sphere ($\rho_2 = 0$), Eqn. 1 simplifies to:

$$\delta\varphi(\mathbf{r}) = \frac{a^3\mathbf{E}_0 \cdot \mathbf{r}}{r^3} \quad (2)$$

For insulators such as plexiglass or quartz, with $\rho_2 >> \rho_1$ and $\varepsilon_2 \leq \varepsilon_1$, Eqn. 1 reduces to:

$$\delta\varphi(\mathbf{r}) = -\frac{a^3\mathbf{E}_0 \cdot \mathbf{r}}{2r^3} \quad (3)$$

The electric field vector, $\mathbf{E}_0$, was measured in the midplane as described in Rasnow and Bower (1996). The electric field at selected object points was interpolated from the measured $\mathbf{E}_0$. The body was outlined in the same experiment, which defined the set $\{\mathbf{r}\}$ of field points for the simulations.

Simulated electric images of ellipsoids. Simulation of asymmetrical objects is far more complicated mathematically. The simplest such object, an ellipsoid, is defined by the surface:

$$\frac{x^2}{a^2} + \frac{y^2}{b^2} + \frac{z^2}{c^2} = 1 \quad (4)$$

The analysis is greatly simplified by making the cross section along one axis symmetrical, e.g., setting a = b. The perturbation potential at a distance $\mathbf{r}$ = (x,y,z) from such a conducting ellipsoid is (modified from Landau et al. 1984):

$$\delta\varphi(\mathbf{r}) = (xE_x + yE_y)\frac{\Psi\left(\frac{u}{v}\right) - \frac{uv}{\xi + a^2}}{\Psi\left(\frac{u}{c}\right) - \frac{uc}{a^2}} - zE_z\frac{\Psi\left(\frac{u}{v}\right) - \frac{u}{v}}{\Psi\left(\frac{u}{c}\right) - \frac{u}{c}} \quad (5)$$

where $\Psi(\upsilon) = \tanh^{-1}(\upsilon)$ for an oblate spheroid (a = b < c) or $\Psi(\upsilon) = \tan^{-1}(\upsilon)$ for a prolate spheroid (a = b > c); E_x, E_y, and E_z are the electric field components at the center; ξ is analogous to the radial spherical coordinate, defined by:

$$\frac{x^2 + y^2}{a^2 + \xi} + \frac{z^2}{c^2 + \xi} = 1 \quad (6)$$

and *u* and *v* are given by:

$$u = \sqrt{\left|a^2 - c^2\right|}, \quad v = \sqrt{c^2 + \xi} \qquad (7)$$

This has a similar form to Eqn. 1, except the dot product, **E**•**r**, contains different scaling factors for each axis, which are complicated functions of the ellipsoid axes, a, b, and c.

The simulations were performed on a Macintosh Centris 660AV computer using Matlab 3.5 software (The Mathworks Inc., Natick, MA). The measurements were made with a Macintosh IIfx computer using Matlab with custom software and hardware (Rasnow 1994).

Results

Waveforms of object perturbations

Figure 1 shows the effect of a brass sphere on the EOD waveform recorded between two electrodes, one positioned against the skin directly lateral of the object, and the second 30 cm lateral of the fish. Even at its nearest distance, where the edge of the 11 mm radius sphere was a mere 2 mm from the skin, the EOD amplitude changed by less than 15 percent. Some distinctive features of these waveforms are that the object does not change the EOD potential by a multiplicative factor. The perturbations (Fig. 1, rows 2 and 4) are not simply proportional to the unperturbed waveforms (top curves, rows 1 and 3). In all four rostrocaudal positions, certain phases are more perturbed than others. Some EOD phases have both invariant and nonzero amplitude with respect to object distance. The relative amplitudes of the double peaks of the EOD and the object perturbation at the tail (Fig. 1D) are also opposite each other. To understand what may cause such nonlinear modulations, I examined the electric field without the object, in the space where the object was placed. It is expected on theoretical grounds (see below and Methods) that the perturbation directly lateral of the object should be proportional to the lateral electric field component at the object.

Figure 2 shows the electric field components in the area of the midplane that was occupied by the sphere. At the head, the waveform of the object modulation (Fig. 2A, lowest curve) is similar to the lateral electric field. At the tail (Fig. 2D), the electric field is much more variable over the area of the object. Of the two positive peaks of the lateral field at D, the first peak is largest at the rostral side of the object and the second peak is dominant caudally. The perturbation caused by the object closely resembles the lateral field waveform near the lower center of the object. The effect a small object has on the EOD at the skin is to add a perturbation, proportional to the electric field at the object. The resulting sum is generally not the same as a constant multiplicative change in the unperturbed EOD.

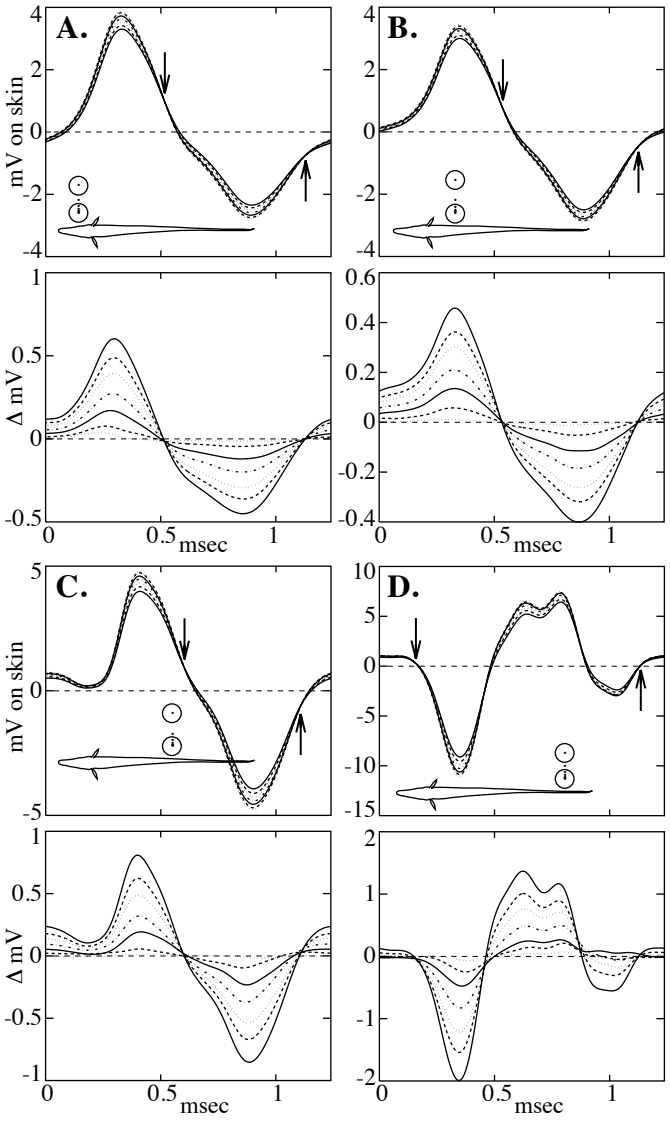

Fig.1. Rows 1, 3. The potential waveforms, recorded between an electrode on the skin lateral of the object, and an electrode 30 cm lateral of the fish. An 11 mm radius brass sphere was located at seven object-fish distances (insets) from 13 to 43 mm lateral of the skin (skin to object-center distance), at 4 rostro-caudal positions (**A-D**). The lowest amplitudes correspond to the object nearest the fish. Rows 2,4. The EOD perturbation due to the object, computed by subtracting the potential with the object present from the potential without the object. Note the perturbation waveforms are not proportional to the unperturbed potential (especially at the tail). The EOD phases that are unaffected by the object (arrows) also have non-zero amplitude.

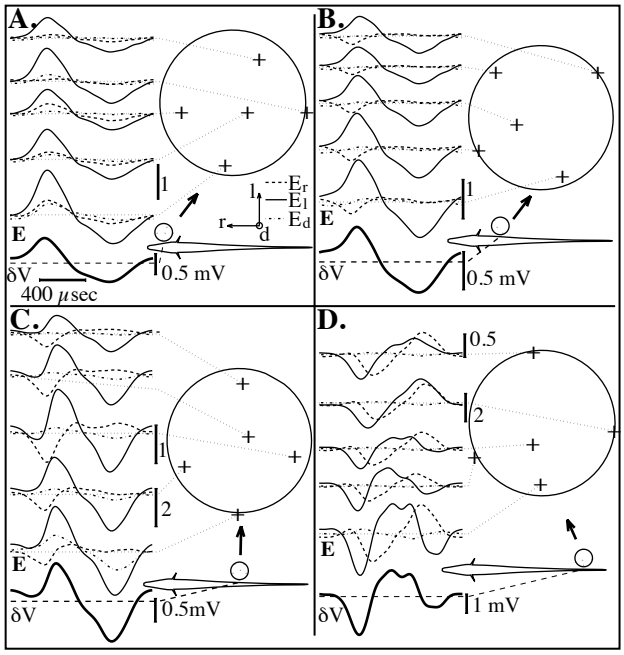

Fig.2. **A** The simulations are based on the unperturbed EOD field at the position of the object. The Cartesian components of the 3-dimensional electric field are shown at several locations within or near where the brass sphere was closest to the fish (units are mV/cm, indicated by vertical scale bars). The potential perturbation, measured on the skin with the object at this position (lowest waveform) is similar to the lateral electric field component (E_l) waveform. The figure is repeated in **B-D** at three other rostrocaudal locations. The electric field becomes much more spatially variable near the tail.

Simulations of object waveforms

The simplest approach to simulate the object perturbation at the skin is to treat the electric field as spatially uniform, with value equal to the unperturbed field at location of the object's center. The perturbation on the skin at the same rostrocaudal position as the center of the object is (from Eqn. 2):

$$\delta\varphi(1) = \frac{a^3 E_l(1)}{l^2} \qquad (8)$$

where l is the lateral distance between the skin and object center, and E_l is the unperturbed lateral electric field component, and *a* is the object's radius. The perturbation is independent of the rostral and dorsal electric field components directly lateral of the object.

Figure 3 shows the simulated and measured waveforms of the object perturbation on the skin at four different rostro-caudal positions (A-D) and at four object-fish distances (insets). The amplitudes of the simulations and measurements are similar, although the waveforms differ slightly. The largest difference between simulation and measurement occurs at the most caudal position with the

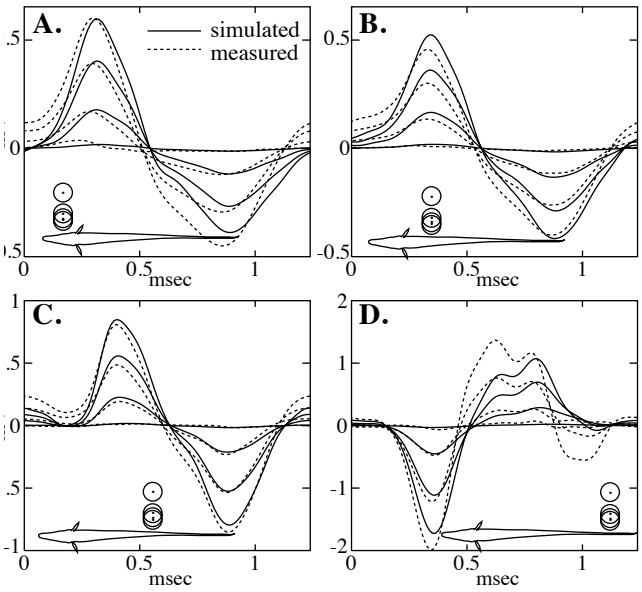

Fig. 3. Simulated and measured potential perturbation waveforms are compared at four rostrocaudal positions (**A-D**). The object was a 11 mm radius brass sphere at distances of 13, 15, 20, and 43 mm between the center of the object and the skin. The average amplitudes generally agree, although the waveforms differ slightly between the two methods.

object nearest the fish, precisely where the electric field is least spatially uniform. If I had used E_l at a point slightly rostral of the object's center for this simulation, there would be closer agreement with the measurements. Note that there are no free parameters in these simulations, and no "optimizations" were performed to reduce the difference between measured and simulated data.

Fourier analysis of the waveforms in Fig. 3 reveals a 12-20° (40-70 μsec) phase lag between the simulated and measured fundamental frequencies at each rostrocaudal location, that is independent of the object-fish distance. The phases of the harmonics tend to agree within a few degrees when the object is nearest the body, but diverge with increasing object distance. However, the amplitudes of the fundamental and all harmonics closely agree. This phase discrepancy suggests that a more sophisticated model of the object and the EOD field is required to accurately predict the phase shifts induced by this metal sphere (see Discussion).

Amplitude vs. lateral distance

The amplitude of the object perturbation as a function of object-fish distance is shown in Fig. 4. The measurements and simulations generally agree over two orders of magnitude. Far from the fish, the electric field is more uniform over the object, and thus the simulation becomes more accurate. However, at increased object distances, the measured object perturbations decrease and thus become more susceptible to noise. At object-fish center-to-center distances greater than approximately 4 cm, the perturbation

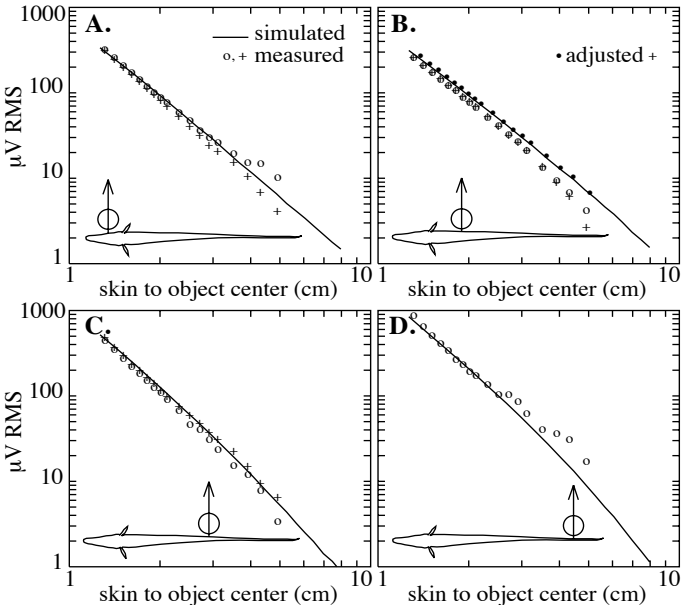

Fig. 4. Simulated and measured RMS amplitude of the potential perturbation on the skin lateral of an 11 mm radius brass sphere, as a function of object-fish distance. The sequence of measurements was repeated twice in **A-C**. In **B,** the dots represent the '+' measurements after two small systematic corrections were applied (see text).

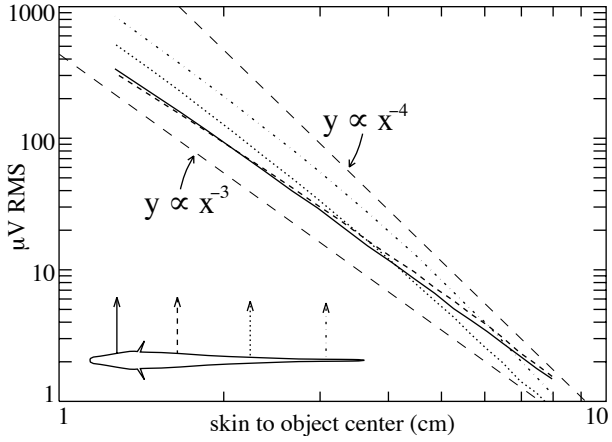

Fig. 5. RMS amplitude of the simulated potential perturbation lateral of an 11 cm radius brass sphere, at four rostrocaudal positions. The amplitudes decay as distance to the –2.9 to -4^{th} power, with larger decay rates caudal and further away from the fish. The left and rightmost dashed lines show decay rates of $1/r^3$ and $1/r^4$ respectively for reference. A sphere closer than 5 cm from the fish produces a larger perturbation lateral of the tail than when equidistant of the head and trunk. Likewise, a sphere further than 7 cm from the tail generates a smaller perturbation than when equidistant from the head or trunk. The perturbation amplitude is proportional to the object's volume, so by just normalizing the vertical scale, this figure applies to any size conducting sphere.

amplitude is less than one percent of the EOD. Therefore the measured perturbation is a small difference between two large measurements, which is an unfavorable condition for data analysis due to error propagation.

The measured perturbations are also extremely sensitive to systematic errors in object position and the unperturbed potential. Measuring absolute distances near the fish to submillimeter resolution, given the optical distortions due to the water, large plexiglass tank, and the object, is a difficult task. In addition, placing the electrode array flush against the fish can push the body slightly away from the object. I explored whether these factors might explain the largest deviation between measurements and simulations, which occurred in Fig. 4B. Systematically adding 0.5 mm to the fish-object distances, and adding 4 μV to the measured 1.85 mV EOD amplitude with the object at infinity (a 0.2% correction), virtually eliminated the discrepancy between measurements and simulations (dots in Fig. 4B).

The simulated data from the four rostrocaudal locations in Fig. 4 are shown together in Fig. 5. For small lateral distances, perturbations from objects at the tail are much larger than for equidistant objects near the head. This is because the electric field is larger near the tail, and the perturbation is proportional to the lateral electric field (Eqn. 8). Like the electric field, the perturbations attenuate more rapidly with lateral distance at the tail. The average decay rate or the slope in Fig. 5 was computed by least squares fit to a power law: perturbation amplitude $\propto$ (fish surface to object center distance)$^{-\gamma}$. The average exponent, γ ranged from 2.9–3.6, with larger values near the tail. For objects beyond several centimeters from the tail, γ is slightly greater than four.

Images along the skin

Thus far I have presented object perturbations at one point on the skin, lateral of the object. Perturbations at other points in the midplane were also measured simultaneously with a 5-electrode array (Fig. 6; Figs. 1, 3-5 are from the central electrode of the array). Although the measurements show considerable variance, they generally agree with the simulations. The electric images broaden as the object recedes from the fish, and the peaks of the images are slightly offset from the location of the object. These phenomena are explored further below (Figs. 8 and 9).

The simulator permits one to dissect the relative contributions of different electric field components to an object's electric image. Fig. 7 shows the simulated electric images of a 10 mm radius conducting sphere at four orientations of the electric field that occur during the EOD cycle (see Rasnow & Bower 1996). Even when the electric field is nearly tangential to the skin (phase 1), there is a finite perturbation. Furthermore, this orientation of the electric field creates the largest amplitude perturbation at the flanks of the electric image, rostral and caudal of the object (arrow in Fig. 7B). The influence of the rostral electric field component is largest rostral and caudal of the object because the local perturbation is:

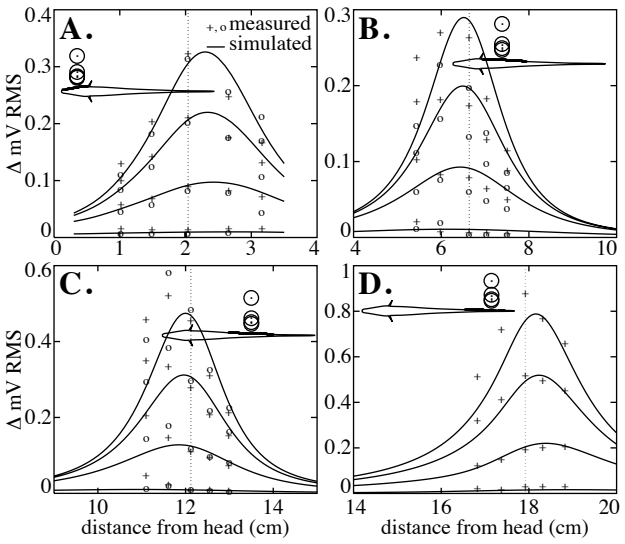

Fig. 6. Simulated and measured potential perturbations for the same object positions as in Fig. 3. The measurements were made with a 5 electrode array on the midline skin and a distant reference electrode. The vertical lines indicate the rostrocaudal locations of the object center. The object was moved through a sequence of lateral distances twice (+, o) in **A-C** to give an indication of variability and sensitivity to errors.

$$\delta\varphi \propto \mathbf{E}\cdot\mathbf{r} \propto E_{rostral}\sin\theta + E_{lateral}\cos\theta \qquad (9)$$

where θ is the angle between the object and the normal vector at the measurement point on the skin. Moving along the body away from the object increases θ and the influence of the rostral field.

The simulator can also predict the object's effect on the electric field or current at the skin (Fig. 7C, D). The field perturbation decays more rapidly with distance from the object than the corresponding potential. Thus the field image is spatially more compressed across the skin. The field and potential images have opposite sign because of the different locations of the reference electrode. A conducting sphere causes a local increase in lateral current and electric field below it. This results in an increased voltage drop over the skin (Ohm's law), and consequently a reduced potential between the outside surface of the skin and the distant reference electrode.

Image shape vs. lateral distance

The peaks of the electric images in Figs. 6 and 7 are displaced along the body relative to the position of the object. Consequently the receptors slightly rostral of the object in Fig. 7 will respond most vigorously. The peak offsets, quantified in Fig. 8, occur because the unperturbed EOD field is not normal to the body. The dipole moment of the perturbation is parallel to the electric field (Eqn. 1). Thus the projections of the dipole lobes have their maxima displaced towards where the field vector intersects the skin. The direction of the average electric field, indicated by

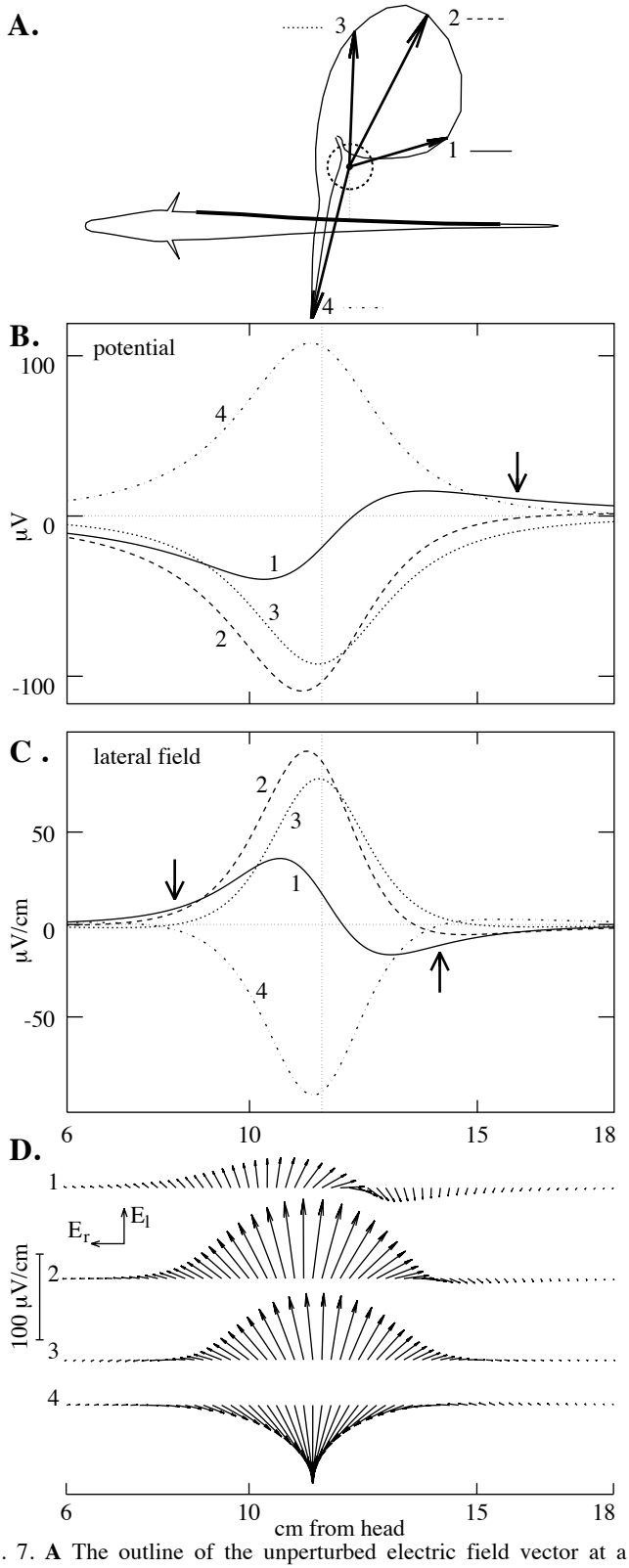

Fig. 7. **A** The outline of the unperturbed electric field vector at a point where the perturbation of a 1 cm radius conducting sphere is simulated. The potential perturbation (**B**) and the perturbation of the lateral electric field (**C**) at the skin at the four EOD phases denoted by arrows in **A**. Even when the electric field at the object is nearly tangential to the skin (phase 1), the perturbations are finite, and in the locations shown by arrows, exceed the perturbations of the other phases. **D** Vector representation of the electric field perturbation during the same four phases of the EOD.

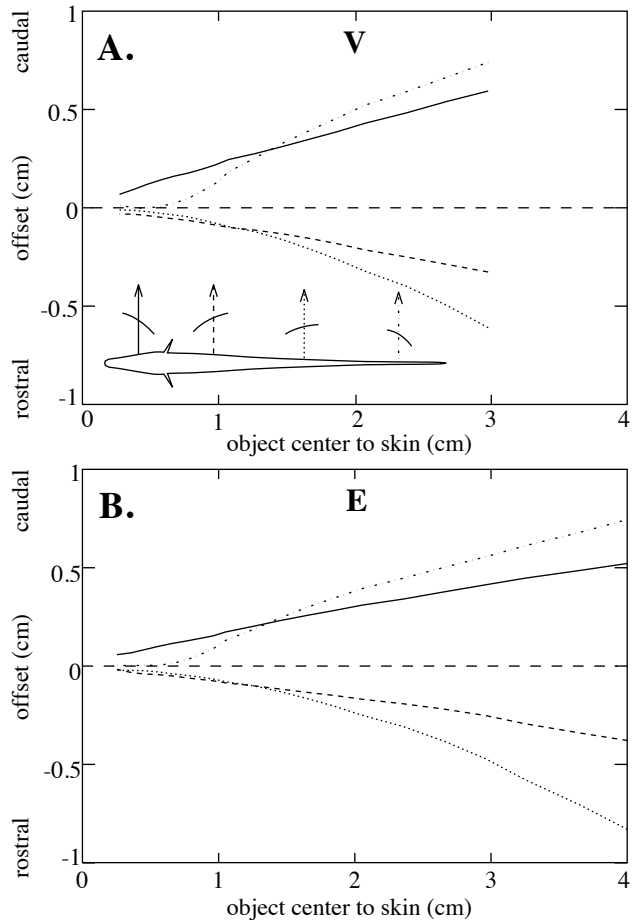

Fig. 8. The location of the electric image peak is slightly offset from the location of the object. The offsets result primarily from the tangential components of the unperturbed electric field at the object, which causes the lobes of the dipolar perturbation to intersect the body rostral and caudal of the object. The average field directions are schematically indicated by curves in the inset. The peak offsets of the potential images (**A**) and field images (**B**) are qualitatively similar. Both increase with object-fish distance, but are small compared to the width of the images (Fig. 9).

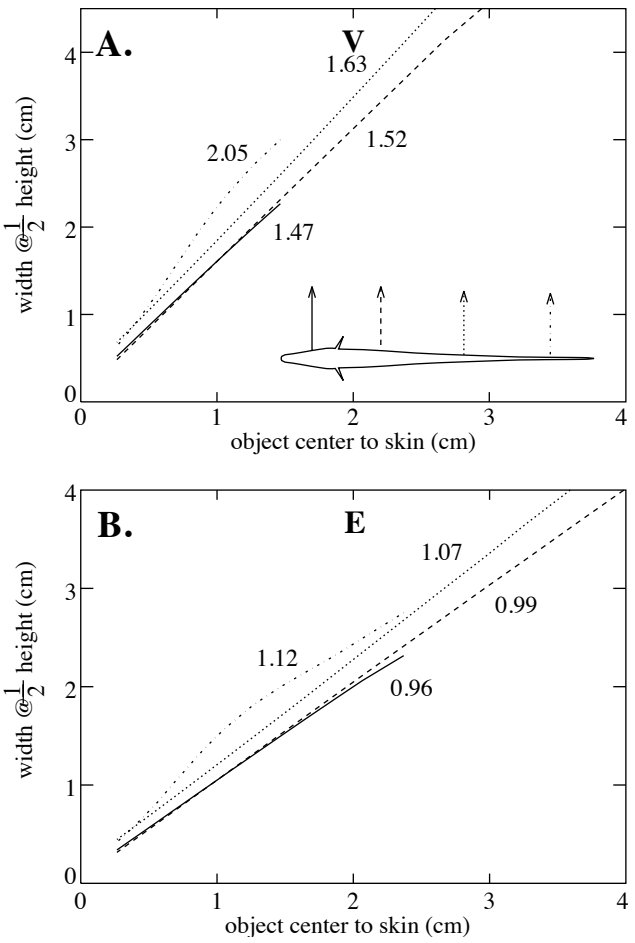

Fig. 9. The width of the electric image at half the peak amplitude increases linearly as the object moves away from the body. The numbers give the slope of the curves at the four rostrocaudal locations. Near the head and tail, the full width at half height is only defined for nearby objects. Measuring the full width at 90% amplitude (not shown) also results in an extremely constant slope. The potential images (A) and field images (B) are again qualitatively similar.

curves in the inset of Fig. 8A (see also Fig. 7 of Rasnow and Bower 1996), is consistent with the peak offsets. The curvature of the body additionally contributes to the offsets, because receptors on the skin where the body curves away from the object detect a more attenuated signal than they would if the body were flat.

Electric images can also be characterized by their broadness or spread across the skin. The width at half of the peak amplitude is a simple measure of this image feature. This parameter is an extremely linear function of object distance near the fish for both potential and field images (Fig. 9). Data is only shown for objects near the fish because for more distant objects, the perturbation at the mouth or tail tip exceeds half the peak amplitude, and thus this measure is not defined. I therefore computed the width at 90% of peak amplitude (not shown), which also increases linearly with nearly constant slope to object-fish distances greater than 5 cm.

The lateral electric field image is both more focused, and widens with object distance more gradually than the potential image (Fig. 9). However, like the potential image, the slope is independent of object distance, and gradually increases monotonically from head to tail. This suggests that the spatial resolution of electric sense could be slightly higher at the head than at the tail, and less variable with object distance. Note that this result holds for any homogeneous spherical object, independent of its radius or impedance. From Eqn. 1, the radius and impedance affect the global amplitude and phase of the image, but not the image's relative width.

Images of ellipsoids

I next examine how the electric images of spheres compare to those of oblate and prolate spheroids with eccentricity e = 2. The ellipsoid volumes in Fig. 10 were

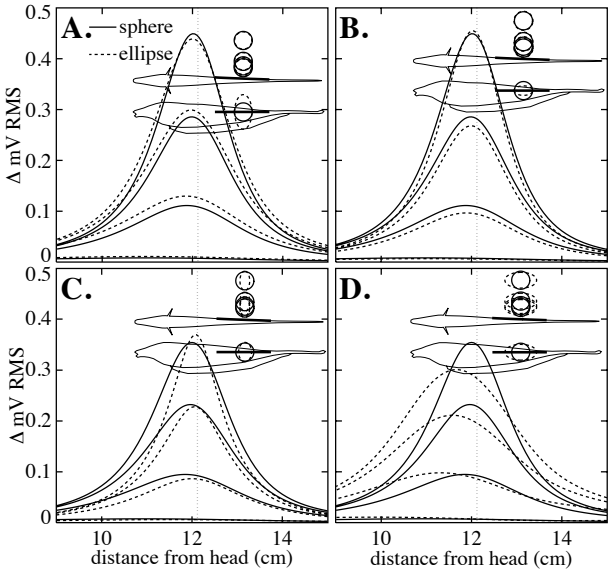

Fig. 10. Comparisons of the electric images of conducting spheres and oblate and prolate spheroids with eccentricity of 2 in various orientations (insets). The volumes of the ellipsoids have been adjusted so the images have similar peak magnitudes as the sphere. **A**, **B** The ellipsoids are oriented with dorsoventral asymmetric axis and the midplane circularcross-section. The resulting images are similar to those of spheres. **C, D** Eccentric midplane cross-sections alter more profoundly the shape of the electric images.

chosen to approximately match the peak image magnitudes of the spheres, in order to facilitate comparisons (the locations of the centers of the spheres and ellipsoids were the same). Ellipsoids with symmetric axes in the midplane generated electric images similar to those of spheres. However, when oriented with elliptical cross-sections in the midplane, several image features change. The narrower and wider cross-sections of the ellipsoids in Fig. 10C and D respectively result in analogous changes in the widths of the electric images. Furthermore, although the volume of the ellipsoid in Fig. 10C is less than in Fig. 10D, the peak amplitude of its image is greater.

Figure 11 shows how ellipsoids respond to different electric field components. Three ellipsoids of equal volume but different orientations were simulated at the same location and EOD phases as in Fig. 7. Each phase of the image of the ellipsoid with circular midplane cross-section is similar to a sphere (Fig. 11A and Fig. 7B). A rostrocaudally flattened ellipsoid (Fig. 11B), in addition to having a more focused image with a lateral field, hardly responds to the rostrocaudally oriented fields. The image at phase 1 is attenuated, and phases 2 and 3, which have similar lateral field components, produce similar images. However, a laterally flattened ellipsoid (Fig. 11C) has a broader and overall attenuated image, except in response to the rostrocaudal electric field. At phase 1, the image is larger than in either Fig. 11A or B. Also the images at phases 2 and 3 are substantially different.

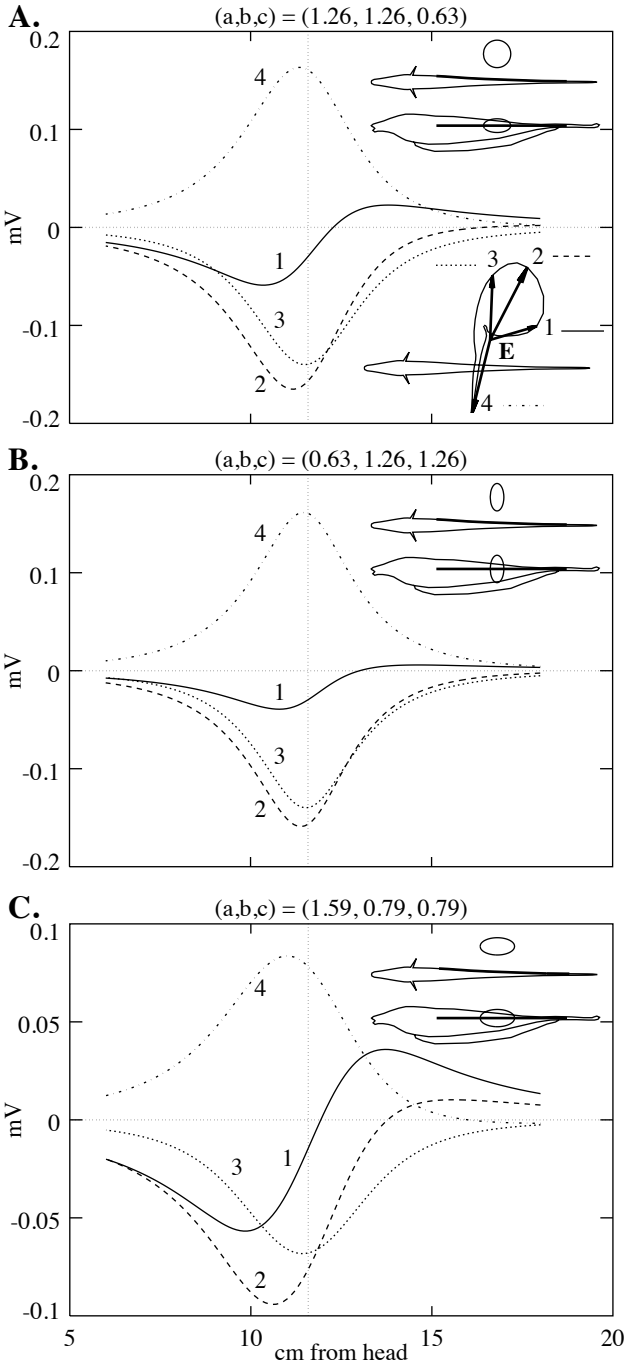

Fig. 11. The instantaneous electric images of three unity volume ellipsoids at the same location and phases as in Fig. 7 (inset, **A**). **A** This ellipsoid has circular midplane cross-section, and the electric images at all phases are similar to those of a sphere (Fig. 7B). **B** This rostrocaudally flattened ellipsoid produces only a weak perturbation to rostrocaudal fields (phase 1). Also the images at phases 2 and 3 are similar. **C** This rostrocaudally elongated ellipsoid produces a strong perturbation during phase 1, and the differences between phase 2 and 3 images is pronounced. Different electric field orientations therefore reveal asymmetry of the objects.

Discussion

In this study, I have attempted to develop an intuition about how weakly electric fish might perceive objects with their high frequency electric sense. Early studies of object perturbations (e.g., Hagiwara & Morita 1963) measured changes in electroreceptor afferent firing rates in response to large moving blocks, plates, or cylinders, near the fish. Although these large objects, and the electroreceptor transfer function, improved the signal-to-noise ratio, the data was too complicated to quantify how individual object parameters might be neurally encoded. Realizing this, Scheich et al. (1973) simplified the perturbations by replacing the fish's (*Eigenmannia*) EOD with an artificial sinusoidal field. These experiments provided novel information about individual electroreceptor transfer functions, but did not address the spatiotemporal properties of electric images. Heiligenberg's (1975) 2-dimensional finite difference simulator provided a first view of electric images, which quantified the low spatial resolution and short range of electric sense. Hoshimiya et al. (1980) used the more powerful finite element algorithm to simulate electric images on a 2-dimensional elliptical "fish". Bacher (1983) constructed a 3-dimensional analytic simulation using a pair of line charges to model the unperturbed EOD, and a dipole for the object. His general solution was in terms of an integral, which I have solved (Eqn. 1, see Appendix for derivation). Bastian (1981) did extensive measurements of perturbation amplitudes and changes in receptor afferent firing rates due to moving spheres and cylinders.

This is the first study to suggest a model of how sets of electric image features, such as peak amplitude, width, and phase shift, might encode important features of objects, such as their size, shape, location, distance, and impedance. An essential step in deriving this model was to define fish-object distance in an unconventional manner. Whereas it is natural experimentally to measure object distance between the skin and the sphere's surface, the sphere's effects have a simpler functional form in terms of the distance to its center–the point of symmetry of its perturbation. Including the sphere's radius in its distance from the fish has a profound influence on the analysis results.

Accuracy of the simulator and measurements

The simulated electric images are the basis for a proposed model of electrolocation. An essential prerequisite was to ascertain the accuracy of the simulator, which was done by comparing the simulations with independent measurements of object perturbations (Figs. 3, 4, and 6). Although I use the terms "simulated" and "measured" to label my two methods of deriving electric images, the simulations are also based on actual measurements of the unperturbed electric field (Rasnow and Bower 1996). Electric field measurements are less sensitive to EOD variance and instrumentation noise because the data is recorded synchronously and differentially. Field measurement errors also propagate through the object simulation without amplification. In contrast, the measured perturbations are much more sensitive to errors. For example, variations in EOD amplitude of only 0.1% during the few minutes that the object was moved from near the fish to infinity result in a 10% uncertainty of a 1% amplitude modulation. Measuring large common mode signals also requires greater precision of the electronic instrumentation, since nonlinearities such as interchannel crosstalk and harmonic distortion are typically proportional to the signal magnitude.

To improve the signal-to-noise ratio of the measured images, I used an 11 mm radius metal sphere for a test object. Even with the edge of this huge conductor just 2 mm from the skin, the potential between the skin below the object and a distant electrode changed by less than 15 percent. Since the object has a large effect on the impedance just outside the fish and the change in potential is relatively small, most of the voltage drop from the EO must occur within the fish. The skin and body of *Apteronotus* have resistivity of approximately 3 kΩ-cm^2 and 300 Ω-cm respectively at the trunk (unpublished measurements and Scheich and Bullock 1974). Therefore, the skin has 10 times the resistance to normal currents as a 1 cm thick slab of body tissue, and by Ohm's law, the voltage drop will be primarily across the skin.

The high resistance of the skin partially insulates the fish's interior from an object perturbation. As a rough approximation, the skin resistance is equivalent to 6 mm of 5 kΩ-cm water (for normal current), and therefore the inside of the skin is effectively 6 mm farther from the object than the outside of the skin. Since a dipole perturbation decays steeply with distance from the object, a nearby object will change the exterior potential much more than the interior potential. However, as the object-skin distance increases, so does the magnitude of the interior perturbation relative to the perturbation outside. Therefore, farther from the object, the potential simulations and measurements overestimate the transdermal perturbation. This explains why the simulated potential perturbations are broader than the corresponding perturbations of the lateral electric field (Fig. 7). The transdermal potential is proportional to the normal field and the skin impedance (Eqn. 10, below). I measured potentials relative to a distant electrode to eliminate trauma and possible distortion of the electric field from inserting an internal reference electrode.

There are two major assumptions in the simulator that are of questionable validity. The unperturbed electric field is assumed uniform over the volume of the object. This is clearly violated, especially near the tail, and to a lesser degree at the trunk and further from the fish (Fig. 2). Had I chosen a smaller object, the electric field would have been more uniform, but the perturbation amplitude would have decreased as the cube of the object radius (Eqn. 1), proportionally reducing the signal-to-noise ratio of the measurements. A nonuniform field induces higher order multipole perturbations, in addition to a dipole moment

proportional to the mean field. Multipoles attenuate with distance from the object more rapidly than the dipole perturbation. Since the measurements generally agree with the dipole simulation, the nonuniformity of the EOD field is of little significance, especially for small objects. The small discrepancies between measurement and simulation might also result from a small error in the location of the object.

A second assumption in the model is that there is no fish, i.e., the perturbation at the skin is not affected by the fish's presence. A 1 cm cubic section through the trunk should have a lateral resistance of approximately $R \approx (1\ cm^2)\ (2\ \rho_{skin} + \rho_{body} * 1\ cm) \approx 6\ k\Omega$. The same size section of water has resistance of 5 kΩ. Since the perturbation is also a small contribution to the overall field, the trunk should exert a relatively minor affect on the simulation result. Other parts of the body may have more notable effects, especially above and below the midplane.

In comparing the object measurements with the simulations, I assumed the brass sphere was a perfect conductor. However metals in water are subject to complicated chemical reactions at their surface that can cause large deviations in their behavior from that of a perfect conductor (Robinson 1968). For example, the metal surface rapidly oxidizes, and the sphere becomes analogous to a leaky capacitor with the water. This may be the cause of the observed phase shift between the measured and simulated waveforms. Although the perturbations from insulating spheres are half the amplitude of conducting ones (Eqn. 3), they should be free of these complex surface phenomena.

In summary, the simulations of object perturbation amplitudes generally agree with measurements to within the uncertainties of the measurements. The simulator accuracy improves with increasing object distance and decreasing object size, precisely the conditions that are most difficult to measure accurately. The simulator is quite robust to the violations of its assumptions even for large objects very close to the fish. Although it does not predict as accurately the phase shifts due to a metal sphere, this may result from the sphere deviating from an ideal conductor.

Range of active electrolocation

There are several ways to characterize the attenuation of electric images with increasing fish-object distance. When fitting the image amplitude to a functional form, such as a power law, $(distance)^{-\gamma}$, the distance can be measured from the skin or midline of the fish, to the edge or center of the object, and each choice results in different values for γ. The dipolar perturbation at the skin due to a sphere has the simplest functional form in terms of distance between the skin and the center of the sphere (Eqn. 1). Using this measure, least squares fit yields γ = 2.9 at the head and trunk, which increases caudally to slightly over 4.0 at lateral distances greater than several cm at the tail (Fig. 5). The decay rate of the lateral electric field, as a power of distance from the fish's *centerline* was shown in Rasnow & Bower (1996) to be $\gamma_E = 1.2$ at the head and 2.0 at the tail. From Eqn. 8, the object perturbation decays proportionally to the lateral field and the inverse square of the distance between the object center and the fish's *skin*. The distance from the skin to the centerline decreases the decay exponent slightly from $\gamma_E + 2$. I also compared these results with those of Bastian (1981). His decay exponents were around 1.2 because he fitted the amplitude to the distance between the skin and object surface. Reanalysis of some of his data (the highest curve in Fig. 8C of Bastian 1981, it is not evident where on the body these data come from), gives a decay rate of 3.1 in my units. Furthermore, this reanalysis causes his data to fit much closer to a power law over the entire range of object distances.

The amplitude of an electric image is proportional to the object volume or the cube of its radius (Eqn. 1). Therefore the data presented for an 11 mm radius sphere can be simply scaled to any size of (small) sphere. For example, replacing the 11 mm radius sphere with a 14 mm radius sphere results in an electric image with twice the amplitude, and likewise an 8.7 mm radius sphere produces an image with half the amplitude.

Although the image amplitude is proportional to the object volume, the rate of attenuation with lateral distance is independent of the radius. Thus for a given object, it should be simple to compute a maximum distance at which its perturbation can be detected by an electroreceptor or the fish. Electroreceptor sensitivity has been estimated from behavioral and electrophysiological studies. However, correlating the perturbation amplitude to electroreceptor stimulus is complicated because the receptors do not respond only to the EOD amplitude. P-receptors adapt to continual stimulus, with a time "constant" of 0.5–3.5 seconds (the adaptation time is not constant but depends on stimulus amplitude; Hopkins 1976). These receptors have other complicated temporal filtering properties (Bastian 1981; Nelson et al. 1993) as well as directional preferences (McKibben et al. 1993). Additionally, electroreceptors are more sensitive than the apparati that have been used to study them, so their thresholds were usually extrapolated from larger perturbations. Thus, electroreceptor thresholds should only be interpreted as rough estimates.

Knudsen (1974) observed behavioral responses to field strengths as low as 0.2 μV p-p/cm in 2 kΩ-cm water, applied between plates lateral of the fish (*A. albifrons*). Although the fish might be sensing this perturbation with its phase coding or T receptors, as well as its amplitude coders or P units, Bastian (1981) measured the physiological responses of single P units to the same stimulus in 10 kΩ-cm water. His extrapolated and estimated threshold field was 0.9 μV p-p/cm. These data can be compared by estimating the corresponding changes in transdermal potentials caused by the imposed fields. By Ohm's law, the change in current density outside the skin is approximately $\Delta J = \Delta E/\rho_{water}$. This current flows across the skin, generating the change in transdermal potential,

$$\Delta V = \Delta J \rho_{skin} = \Delta E \frac{\rho_{skin}}{\rho_{water}}. \quad (10)$$

Estimating ρ_{skin} = 3 kΩ-cm^2, the behavioral and physiological thresholds both correspond to a 0.3 μV p-p or 0.1 μV RMS change in transdermal potential. This value is much lower than other estimates of receptor thresholds in *Apteronotus*. For example, Hopkins (1976) found a field of 20 μV/cm or more was needed to cause a perceptible change in an electroreceptor firing rate. However, the stimulus condition in this experiment was much different, and more artificial: the EOD was silenced and replaced by a single frequency sine wave.

It is more accurate to consider smaller objects than to extrapolate Fig. 5 to distances corresponding to a 0.1 μV perturbation. A 5 mm radius sphere has 1/10 the volume of an 11 mm sphere. Therefore a 5 mm sphere generates a 0.1 μV perturbation at the same distances that the 11 mm sphere generates a 1 μV perturbation: approximately 9 cm lateral of the head and trunk, and 8 cm lateral of the tail. A 1.1 mm radius sphere generates a 0.1 μV perturbation at the same distances that the 11 mm sphere generates a 100 μV perturbation: 2 cm lateral to the head and trunk and 2.5 cm lateral of the tail. If electroreceptor differential thresholds are constant from head to tail, large objects would be detectable farther lateral of the head than tail, and small objects would be detectable farther lateral of the tail than head.

Rostrocaudal differences

Several parameters differ between the rostral and caudal regions of the fish. At the tail, the field is larger and less uniform, has more temporal harmonics, has more rotational components, and decays faster than at the head and trunk (Rasnow and Bower 1996). Therefore electric images of small objects at the tail have greater amplitude, greater width across the body, and attenuate faster with lateral distance. The electroreceptor density also decreases nearly monotonically from head to tail (Carr et al. 1982), as does the corresponding area of the ELL somatotopic maps where the electroreceptor afferents terminate (Shumway 1989). It is difficult to attribute functional significance to these differences without knowing more about the respective electroreceptor populations. As suggested by Rasnow et al. (1993), the order of magnitude larger EOD at the tail requires that caudal electroreceptors have different sensitivities and/or spontaneous firing rates. The steeper attenuation of perturbations likewise implies rostrocaudal differences in gain and/or dynamic range as well. Because of the uncertainty in electroreceptor thresholds, it is difficult to even conclude whether the range of active electrolocation is the same or different across the body for a given sized object. Although I propose here that distant large objects generate smaller perturbations at the tail than at the trunk, differences in receptor thresholds or receptor convergence in the nervous system could compensate for these effects, as could the fish's behavior. Electric fish can wag their tails at much higher lateral velocities than they move their bodies. Such fish-object relative motion could cause higher frequency amplitude modulations, which the receptors are more sensitive to (Bastian 1981).

Localization of objects

The shape or relative amplitudes of electric images on the skin are independent of a sphere's radius (Eqn. 1). Therefore the images shown in Fig. 6 will be the same, within a vertical scale factor, for a range of sphere sizes. Compared to vision, electric images are extremely fuzzy, and the fish can increase the resolution by moving closer to the object. Whereas this was qualitatively demonstrated by Heiligenberg (1975), Fig. 9 shows that the size of electric images increases linearly with increasing object-skin distance. The slope is extremely constant especially over the rostral part of the body. This suggests a very simple algorithm for determining a spherical object's distance, and resolving the difference between a nearby small sphere and a more distant and larger one. The fish would only need to determine the width of the electric image at a particular amplitude relative to the peak. Since fish-object distance may be one of the most important parameters to a fish, I suggest that physiologists look for neurons within the electrosensory tract that encode these features.

The rostrocaudal location of an object is another parameter of critical importance. Fig. 8 shows that the peaks of the electric image lie within a few mm of the rostrocaudal position of the sphere. The offset increases gradually with increasing object distance, however it is always a fraction of the electric image width. For example, the image width at half height from a sphere 3 cm from the fish is 3 cm (Fig. 9B), and the maximum offset of the peak relative to the object position is 0.5 cm (Fig. 8B). Thus objects are approximately located radial of the peak in electroreceptor activity, and the offset decreases as the fish approaches the object. In principle, the fish's central nervous system could compensate for the offsets. The computations would account for the direction of the unperturbed electric field, the already established object's distance, and the local body curvature.

Nonconducting objects

Thus far I have focused attention on the electric images of conducting spheres. However the simulator permits exploration of the effects of spheres with other electrical properties. Eqn. 3 describes the perturbation due to typical insulators such as most (spherical) rocks, with $\rho_2 >> \rho_1$ and $\varepsilon_2 \leq \varepsilon_1$. The perturbation has opposite sign and half the amplitude relative to ideal conductors. If the fish's environment contained only ideal conducting and insulating spheres, the sign of the perturbation could be used to determine the object's impedance. The proposed algorithm

for determining the object's distance is equally applicable to nonconductors because it depends only on relative amplitudes and their locations. Knowing the conductivity and distance, the object's size could be determined from the magnitude of the peak perturbation.

Objects with time constants ($\tau = \rho\varepsilon$) of the order of the EOD period may produce intermediate magnitudes and phase shifts. Therefore based on the perturbation amplitude of the fundamental frequency alone, impedance and size are confounded. For example, a large sphere with impedance slightly different from the water could have a similar dipole moment fundamental amplitude as a smaller sphere with a greater difference in impedance. The phase of the perturbation, and the perturbation amplitudes of the EOD harmonics, however would be different in these two cases. Weakly electric fish are extremely sensitive to phase and temporal shifts in their EOD. Thresholds as low as 0.4 μsec have been measured in some species (Rose and Heiligenberg 1985), which could in principle resolve these differences.

The literature contains sparse references to the electrical properties of aquatic objects that electric fish encounter naturally. Many biological objects have huge dielectric strengths, because of their thin membranes and high concentrations of polar molecules. Heiligenberg (1975; 1989) measured the resistivity and capacitance of the leaves of an aquatic plant that provide camouflage for *Eigenmannia*. *Hygrophilia* has resistivity ρ_2 = 200 kΩ-cm, capacitance C = 76 nF/cm^2, and a thickness of 0.2 mm. This corresponds to a dielectric constant ε_2 = 1.6 nF/cm. Imagining a spherical "leaf" of this material, in water with ρ_1 = 5 kΩ-cm and $\varepsilon_1 = 80\varepsilon_0$ = 7 pF/cm, the perturbation becomes (from Eqn. 1):

$$\delta\varphi(\mathbf{r}) = \frac{a^3\mathbf{E}_0\cdot\mathbf{r}}{r^3}\left(\frac{-195 + i10.1f}{405 + i\,10.1f}\right) \qquad (11)$$

where f is the harmonic frequency in kHz. At the 800 Hz fundamental frequency of my *A. leptorhynchus*, the term in parenthesis becomes –0.48 + 0.03i, only slightly different from a rock (a 3.5 degree phase shift). The lowest *k* harmonics are shifted by approximately 3.5*k* degrees. This result does not imply that *Hygrophilia* has insignificant effect on EOD phase, for the geometry of actual leaves may considerably increase their capacitive effects.

The phase shift of "spherical *Hygrophilia*" becomes much larger in higher resistivity water. Seasonal variation in rainfall cause water resistivity changes of several orders of magnitude. *A. leptorhynchus* normally experiences water resistivity between 2 kΩ-cm in the dry season to 100 kΩ-cm in the rainy season (Knudsen 1974). In 50 kΩ-cm water, the complex term in Eqn. 11 becomes –0.29 + 0.23i at 800 Hz, or in polar coordinates, –0.37 at a phase of 38°. The strong dependence of the phase shift on water conductivity suggests that the electric images of certain objects may dramatically change with seasonal periodicity, and even change over hours due to heavy rains. Von der Emde (1993) independently discovered this sensitivity to water conductivity by measurements of electroreceptor responses in a mormyrid. These variable phase shifts raise questions about whether and how electric fish may achieve invariant perceptions of polarizable objects.

Nonspherical objects

Electric images of ellipsoids with circular cross sections in the midplane are similar to those of spheres (Figs. 10 and 11). In fact, examination of Eqns. 1 and 5 reveals that the shapes of the images of spheres and this class of ellipsoids are identical along the midline, although they differ above and below the midline. Ellipsoids with other orientations produce different images than a sphere, even on the midline. This is because each electric field component is perturbed differently by the ellipsoid, which can be understood intuitively as follows. The major axis of a conducting ellipsoid short circuits a larger region of water than does the ellipsoid along its minor axis. Therefore, the electric field component parallel to the major axis generates a larger perturbation than does the field component parallel to the minor axis. Since different field components probe different cross sections of objects, a fish might obtain three-dimensional information about an object by varying the direction of its electric field.

Although the electric images of the ellipsoids in Fig. 10C and D are not exactly the same shape as those of a sphere, their width and peak offset are approximately consistent with images of smaller and nearer spheres in Fig. 10C and larger and more distant spheres in Fig. 10D. This interpretation is qualitatively correct in terms of the edge or profile of the object nearest the fish. Consider momentarily the large object as composed of many adjacent smaller ones. The parts of the composite object nearest the fish produce disproportionately larger contributions to the composite electric image because of the rapid attenuation with distance. Therefore, electric fish might perceive objects with a spatial distortion that enhances the nearest parts, somewhat analogous to the perspective distortion inherent in wide-angle optical lenses.

The distance between the skin and proximal edge of an object is probably a more important parameter to the fish than the distance to the object's center. The proximal distance can be computed by subtraction of two previously derived quantities: the distance to the object's center and the object's radius. This determination of the proximal distance is even accurate for the ellipsoids in Fig. 10C and D, in spite of the distorted estimates of radius and central distance, because the difference cancels the respective distortions.

Other electrolocation cues

Identification of arbitrary objects from transdermal electric images will necessarily require more complex algorithms than those presented above. Although it is not yet known to what extent electric fish can discriminate

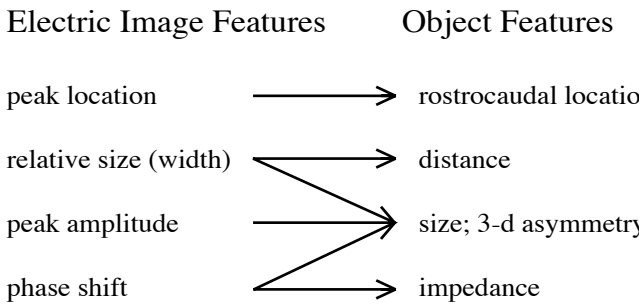

Fig. 12. Summary of the proposed mapping between sets of electric image features and object features.

objects based on their shape and impedance, any such discrimination will require extracting additional parameters from the object's electric images. For example, whereas a sphere can be uniquely located in space by specifying four scalar parameters, such as its radius and the 3-dimensional location of its center, an ellipsoid requires two additional parameters defining the eccentricity.

My proposed mapping of some primary features of electrosensory space to the real space of objects is summarized in Fig. 12. I have shown that the amplitude and shape of an electric image are sufficient to estimate the size, location, and distance, of a simple object. Furthermore, the object's impedance and some degrees of asymmetry can be extracted from phasic features of single electric images. However, electric images contain several other features that could provide additional information about the objects. Probably most important is the temporal sequence of electric images that result from the fish's motion relative to the object. Electric fish explore actively by moving their bodies and tails around objects (Toerring and Belbenoit 1979). The sensory consequences of such motion are likely to be profound, given the strong dependence of the images on the object's distance and rostrocaudal location (Fig. 5). Electric images above and below the midplane also likely reflect the object's shape and asymmetry along the dorsoventral axis. Our lab is working to quantify these issues, as well as trying to establish with behavioral assays the limitations of a fish's electric perception.

Appendix: A Sphere in a Uniform Electric Field

The perturbation due to a sphere in a uniform electric field can be solved as a boundary value problem. Figure 13 shows the idealized problem. A sphere of radius a, with dielectric constant ε_2 and resistivity ρ_2, is located at the origin in a uniform horizontal electric field of magnitude E_o. The sphere is surrounded by media with dielectric constant ε_1 and resistivity ρ_1. I wish to solve for the electric field at a point **r** in region 1. There are no free

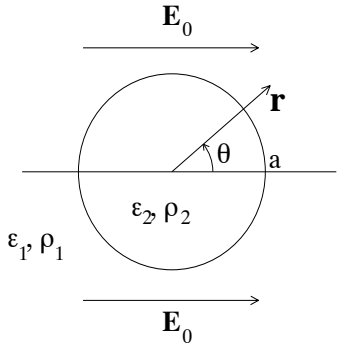

Fig. 13. A sphere with dielectric constant ε_2 and resistivity ρ_2 is in media with dielectric constant ε_1 and resistivity ρ_1 and a unifrom electric field, $\mathbf{E}_0$. I seek a solution for the perturbed potential at a point, **r**, outside the sphere.

charges near the sphere, thus I seek a solution to Laplace's equation and boundary conditions:

$$E_{1\tan} = E_{2\tan} \quad \text{and}$$

$$g_1 E_{1r} + \varepsilon_1 \frac{\partial E_{1r}}{\partial t} = g_2 E_{2r} + \varepsilon_2 \frac{\partial E_{2r}}{\partial t}$$

where $g = 1/\rho$ is the conductivity. Because of azimuthal symmetry, the potential in each domain can be written as Legendre series. Additional constraints are the potential at the origin must be finite. The perturbation from the sphere must tend towards zero at infinity, while the potential gradient approaches $\mathbf{E}_o$. These constraints force all the terms in the Legendre series to zero except:

$$\varphi_1(r,\theta) = -E_0 r\cos\theta + \frac{C}{r^2}\cos\theta \qquad \varphi_2(r,\theta) = Ar\cos\theta$$

The two remaining constants are solved by the two boundary conditions at the surface of the sphere:

$$E_{1\tan} = E_{2\tan} = -\frac{\partial\varphi}{\partial\theta} \Rightarrow -E_0 a + \frac{C}{a^2} = Aa \Rightarrow A = \frac{C}{a^3} - E_0$$

The second boundary condition can be simplified by assuming the potential (and $\mathbf{E}_o$) have sinusoidal time dependence:

$$\varphi(\mathbf{x},t) = \varphi(\mathbf{x})e^{i\omega t}$$

The equations can be solved independently for multiple frequencies. The boundary condition reduces to:

$$\left(g_1 + i\omega\varepsilon_1\right)\frac{\partial\varphi_1}{\partial r}\bigg|_{r=a} = \left(g_2 + i\omega\varepsilon_2\right)\frac{\partial\varphi_2}{\partial r}\bigg|_{r=a}$$

Defining $\xi = 1 + i\omega\varepsilon\rho$ simplifies the algebra, with the result:

$$C = \frac{\rho_1\xi_2 - \rho_2\xi_1}{2\rho_2\xi_1 + \rho_1\xi_2} E_0 a^3$$

or substituting back:

$$C = \frac{\rho_1 - \rho_2 + i\omega\rho_1\rho_2(\varepsilon_2 - \varepsilon_1)}{2\rho_2 + \rho_1 + i\omega\rho_1\rho_2(2\varepsilon_1 + \varepsilon_2)} E_0 a^3$$

and finally, the perturbation due to the sphere is given by:

$$\delta\varphi(\mathbf{r}) = \mathbf{E}_0 \cdot \mathbf{r}\left(\frac{a}{r}\right)^3 \frac{\rho_1 - \rho_2 + i\omega\rho_1\rho_2(\varepsilon_2 - \varepsilon_1)}{2\rho_2 + \rho_1 + i\omega\rho_1\rho_2(2\varepsilon_1 + \varepsilon_2)}$$

This is the potential of a dipole with complex amplitude or phase shift. Simplification for special cases of ε and ρ are treated in the Methods section.

Acknowledgments. I thank Chris Assad for his thoughtful comments and numerous personal and scientific contributions to this work. Jim Bower provided generous support and review of the manuscript. I especially am grateful, and wish to dedicate this paper in remembrance of Walter Heiligenberg, who's encouragement and perspective are dearly missed. This work was funded in part by NSF IBN-9319968.

References

Bacher M (1983) A new method for the simulation of electric fields generated by electric fish and their distortions by objects. Biol Cybern 47:51-58

Bastian J (1981) Electrolocation I. How the electroreceptors of *Apteronotus albifrons* code for moving objects and other electrical stimuli. J Comp Physiol 144:465-479

Bastian J (1986) Electrolocation. In: Bullock TH and Heiligenberg W (eds) Electroreception. Wiley & Sons, New York, pp 577-612

Bastian J (1994) Electrosensory organisms. Physics Today 47:30-37

Bennett MVL (1971) Electroreception. In: Hoar WS and Randall DH (eds) Fish Physiology. Academic Press 493-574

Bennett MVL and Shosaku O (1986) Ionic mechanisms and pharmacology of electroreceptors. In: Bullock TH and Heiligenberg W (eds) Electroreception. Wiley & Sons, New York, pp 157-182

Bullock TH and Heiligenberg W (1986) Electroreception. Wiley & Sons, New York

Carr CE (1990) Neuroethology of electric fish. BioScience 40:259-267

Carr CE, Maler L, Sas E (1982) Perhpheral organization and central projections of the electrosensory nerves in gymnotiform fish. J Comp Neurol 211:139-153

Hagiwara, S and Morita, H (1963) Coding mechanisms of electroreceptor fibers in some electric fish. J Neurophysiol 26:551:567

Heiligenberg W (1973) Electrolocation of objects in the electric fish, *Eigenmannia* (Rhamphichthyidae, Gymnotoidei). J Comp Physiol 87:137-164

Heiligenberg W (1975) Theoretical and experimental approaches to spatial aspects of electrolocation. J Comp Physiol 103:247-272

Heiligenberg W (1989) Coding and processing of electrosensory information in Gymnotiform fish. J Exp Biol 146:255-275

Hopkins CD (1976) Stimulus filtering and electroreception: tuberous electroreceptors in three species of gymnotid fish. J Comp Physiol 111:171-207

Hoshimiya N, Shogen K, Matsuo T, Chichibu S (1980) The *Apteronotus* EOD field: waveform and EOD field simulation. J Comp Physiol 135:283-290

Kalmijn AJ (1986) Detection of weak electric fields. In: Atema J, Fay R, Popper A, Tavolga W (eds) Sensory biology of aquatic animals. Springer Verlag 151-186

Knudsen EI (1974) Behavioral thresholds to electric signals in high frequency electric fish. J Comp Physiol 91:333-353

Landau LD, Lifshitz EM, Pitaevskii LP (1984) Electrodynamics of Continuous Media. 2nd Ed., Pergamon Press, Oxford

McKibben JR, Hopkins CD, Yager DD (1993) Directional sensitivity of tuberous electroreceptors: polarity preferences and frequency tuning. J Comp Physiol 173:415-424

Nelson ME, Payne JR, Xu Z (1993) Modeling and simulation of primary electrosensory afferent response dynamics in the weakly electric fish, *Apteronotus leptorhynchus*. J Comp Physiol 173:746

Paulin M (1995) Electroreception and the compass sense of sharks. J Theor Biol *in press*.

Rasnow B, Bower JM (1996) The electric organ discharges of the Gymnotiform fishes: I. *Apteronotus leptorhynchus*. J Comp Physiol *Submitted*.

Rasnow B (1994) The electric field of a weakly electric fish. Ph. D. Thesis, California Institute of Technology, University Microfilms

Rasnow B, Assad C, Bower JM (1993) Phase and amplitude maps of the electric organ discharge of the weakly electric fish, *Apteronotus leptorhynchus*. J Comp Physiol 172:481-491

Robinson DA (1968) The electrical properties of metal microelectrodes. Proc. IEEE 56:1065-1071

Rose G, Heiligenberg W (1985) Temporal hyperacuity in the electric sense of fish. Nature 318:178-180

Scheich H, Bullock TH, Hamstra RH (1973) Coding properties of two classes of afferent nerve fibers: high-frequency electroreceptors in the electric fish, *Eigenmannia*. J Neurophys 36:39-60

Scheich H and Bullock TH (1974) The detection of electric fields from electric organs. In Fessard A (Ed) Handbook of sensory physiology. Springer-Verlag, pp 201-256.

Shumway CA (1989) Multiple electrosensory maps in the medulla of weakly electric gymnotifrom fish. I. Physiological differences. J Neurosci 9:4388-4399.

Toerring MJ, Belbenoit P (1979) Motor programmes and electroreception in mormyrid fish. Behav Ecol Sociobiol 4:369-379

von der Emde G (1993) The sensing of electrical capacitances by weakly electric mormyrid fish: effects of water conductivity. J Exp Biol 181:157-173

von der Emde G (1990) Discrimination of objects through electrolocation in the weakly electric fish, *Gnathonemus petersii*. J Comp Physiol 167:413-421